Engineering Analysis with Boundary Elements 117 (2020) 157–166

Contents lists available at ScienceDirect

Engineering Analysis with Boundary Elements

journal homepage: www.elsevier.com/locate/enganabound

# A dual interpolation Galerkin boundary face method for potential problems

Jianming Zhang[a,*], Le Yang[a], Yijun Liu[b], Weicheng Lin[a], Rui He[a]

[a] State Key Laboratory of Advanced Design and Manufacturing for Vehicle Body, Hunan University, Changsha 410082, China
[b] Department of Mechanics and Aerospace Engineering, Southern University of Science and Technology, Shenzhen 518055, China

ARTICLE INFO

*Keywords:*
Dual interpolation method
Galerkin boundary face method
Moving least-squares approximation
Symmetric BEM
Steady-state potential problem

ABSTRACT

A dual interpolation Galerkin boundary face method (DiGBFM) is applied in this paper by combining the newly developed dual interpolation method with the Galerkin boundary face method (BFM). The dual interpolation method unifies the conforming and nonconforming elements in the BFM implementation. It classifies the nodes of a conventional conforming element into virtual nodes and source nodes. Potentials and fluxes are interpolated using the continuous elements in the same way as conforming BFM, while boundary integral equations (BIEs) are collocated at source nodes, in the same way as nonconforming BFM. In order to arrive at a square linear system, we provide additional constraint equations, which are established by the moving least-squares (MLS) approximation, to condense the degrees of freedom relating to virtual nodes. Compared with the traditional symmetric Galerkin boundary element method (BEM), the symmetry feature of the DiGBFM equations is obtained simply through matrix manipulations, because of the use of the symmetric BEM, and no hypersingular BIE is needed in the DiGBFM. The proposed method has been implemented successfully for solving 2-D steady-state potential problems. Several numerical examples are presented in this paper to show the convergence and accuracy of this new method.

## 1. Introduction

The boundary integral equation (BIE) or boundary element method (BEM) [1–5] are now well-established numerical techniques for solving complicated engineering problems, such as fracture mechanics problems [6–11], wave propagations problems [12], dynamic crack problems [13,14] and frictional contact problems [15].

In many implementations of BEM, the Galerkin scheme is usually applied for symmetry of the matrix which can be used to reduce the computer effort for the Gaussian elimination operation [16]. The symmetric Galerkin BEM was first proposed by Sirtori [17]. One of the main problems for Sirtori's formulation is that one has to solve the hypersingular integrals appeared [18]. L.J. Gray developed this approach to avoid the difficulties inherent with $C^1$ interpolations demanded by a collocation approximation for hypersingular equations by employing non-conforming elements [19]. However, when using non-conforming elements, internal collocation results in a physically unappealing discontinuous interpolation [20]. In addition, very often the traditional symmetric Galerkin BEM is used to solve difficult problems. Against this background, development of the nonconforming symmetric Galerkin BEM's formulation is necessary.

Recently, the first author and his group proposed a dual interpolation boundary face method (DiBFM) [21–23], which has the strong ability to improve the accuracy of nonconforming elements in the BEM implementation. In this method, the BIE is discretized by the dual interpolation element which includes source nodes and virtual nodes. While only the source nodes of each dual interpolation element are taken as the collocation points, that is to say, the BIEs are collocated at source nodes in the same way as nonconforming boundary face method (BFM). In order to make the linear equations system solvable, we provide additional constraint equations, which are established by the moving least-squares (MLS) approximation, to condense the degrees of freedom relating to virtual nodes. Thus, for the same number of source nodes, the final coefficient matrix in the DiBFM is the same size as that in the traditional BEM, while the DiBFM can yield much higher computational accuracy.

Besides, in the DiBFM, both boundary integration and MLS are directly performed on boundary faces, which are described as the form of parametric spaces, and the form of parametric spaces is definitely the same as the boundary representation (B-rep) data structure in actual solid modeling. That is, the geometric data, such as coordinates, outward normal and Jacobians, are calculated directly from bounding curves and bounding surfaces rather than from elements [24] and [25]. Thus, no geometric approximations are introduced in the DiBFM. However, there are two defects of BFM: (i) To obtain the parametric equations of complex models is time-consuming; (ii) The parametric equations need to be used repeatedly to obtain geometric information, the DiBFM requires much more computing effort than the BEM. However,

* Corresponding author.
*E-mail address:* zhangjianm@gmail.com (J. Zhang).

https://doi.org/10.1016/j.enganabound.2020.03.024
Received 26 February 2019; Received in revised form 6 March 2020; Accepted 27 March 2020

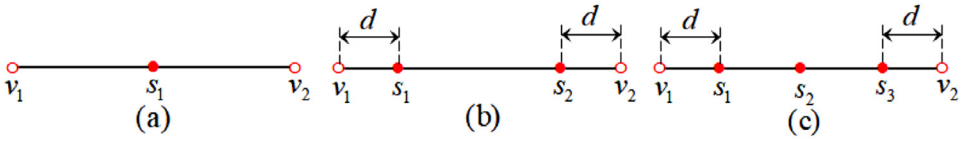


**Fig. 1.** Dual interpolation elements for 2D problems: (a) constant, (b) linear, and (c) quadratic.

the DiBFM still gains higher efficiency for the same level of accuracy. Considering the advantages of the Galerkin BEM [18] in accuracy and in dealing with symmetric matrices, it is natural to extend the Galerkin BEM approach to the dual interpolation BFM.

In this paper, the dual interpolation method is combined with a Galerkin boundary face method (DiGBFM) for solving 2-D steady-state potential problems. This paper extends the results from Ref. [22]. The primary contributions of this paper are as follows: In this new method, (i) the symmetry of the matrix is obtained simply through matrix manipulation, and no hypersingular BIE is employed [26], therefore, this symmetric DiGBFM is easier to implement than the traditional symmetric Galerkin BEM, and it can also reduce the computational cost; (ii) the way of DiGBFM to condense the degrees of freedom relating to virtual nodes is different from that of traditional DiBEM, if we rigidly follow the formulations from Ref. [22], the symmetry of the final coefficient matrix cannot be obtained.

The paper is organized as follows: In Section 2, the dual interpolation method for 2-D steady-state potential problems is introduced. In Section 3, the formulations of the DiGBFM are presented. In Section 4, numerical examples are provided to demonstrate the convergence and accuracy of the proposed DiGBFM in solving 2-D potential problems. In Section 5, we conclude the paper with some discussions.

## 2. Dual interpolation method for steady-state potential problems

It should be mentioned that most equations presented in this subsection can be found in the previous work but reproduced here for the sake of completeness.

### 2.1. Dual interpolation element

The elements in the DiBFM are called dual interpolation elements. As is illustrated in Fig. 1, the dual interpolation elements are divided into different element types. The nodes of a dual interpolation element are classified into two groups: the source nodes (shown as solid red dots in Fig. 1) and the virtual nodes (red circles in Fig. 1). Considering both virtual and source nodes, the element is equivalent to a standard continuous element. Ignoring virtual nodes, it becomes a conventional discontinuous element with a lower order. Thus, the dual interpolation elements have capability on unifying the conforming and nonconforming elements. Shape functions of the elements of type (a), (b), and (c) are given by:

$$N_1^s(\xi) = (1+\xi)(1-\xi) \text{and} \begin{cases} N_1^v(\xi) = \frac{1}{2}\xi(\xi-1) \\ N_2^v(\xi) = \frac{1}{2}\xi(\xi+1) \end{cases}, \tag{1}$$

$$\begin{cases} N_1^s(\xi) = \frac{[\xi-(1-d)](\xi+1)(\xi-1)}{2d(1-d)(2-d)} \\ N_2^s(\xi) = -\frac{[\xi+(1-d)](\xi+1)(\xi-1)}{2d(1-d)(2-d)} \end{cases} \text{and} \begin{cases} N_1^v(\xi) = -\frac{[\xi+(1-d)][\xi-(1-d)](\xi-1)}{2d(2-d)} \\ N_2^v(\xi) = \frac{[\xi+(1-d)][\xi-(1-d)](\xi+1)}{2d(2-d)} \end{cases}, \tag{2}$$

$$\begin{cases} N_1^s(\xi) = -\frac{[\xi-(1-d)](\xi+1)(\xi-1)\xi}{2d(2-d)(1-d)^2} \\ N_2^s(\xi) = \frac{[\xi+(1-d)][\xi-(1-d)](\xi+1)(\xi-1)}{(1-d)^2} \\ N_3^s(\xi) = -\frac{[\xi+(1-d)](\xi+1)(\xi-1)\xi}{2d(2-d)(1-d)^2} \end{cases} \text{and} \begin{cases} N_1^v(\xi) = \frac{[\xi+(1-d)][\xi-(1-d)](\xi-1)\xi}{2d(2-d)} \\ N_2^v(\xi) = \frac{[\xi+(1-d)][\xi-(1-d)](\xi+1)\xi}{2d(2-d)} \end{cases}, \tag{3}$$

respectively, where $\xi$ represents the natural coordinates ranging from -1 to 1 on the element, and the distance $d$ is taken to be $\frac{1}{4}$ in this study. These Equations that are formed by Lagrangian interpolation formulation are also available in Ref. [22].

### 2.2. First-layer interpolation

For 2-D steady-state potential problems, the independent physical variables on the boundary are the unknown potential $u$ and normal flux $q$. These physical quantities are estimated by dual interpolation elements (first-layer interpolation):

$$u(x_1,x_2) = u(\xi) = \sum_{\alpha=1}^{n\alpha} N_\alpha^s(\xi)u(Q_\alpha^s) + \sum_{\beta=1}^{n\beta} N_\beta^v(\xi)u(Q_\beta^v), \tag{4}$$

$$q(x_1,x_2) = q(\xi) = \sum_{\alpha=1}^{n\alpha} N_\alpha^s(\xi)q(Q_\alpha^s) + \sum_{\beta=1}^{n\beta} N_\beta^v(\xi)q(Q_\beta^v), \tag{5}$$

where $n\alpha$ and $n\beta$ are the total number of source and virtual nodes of a dual interpolation element, respectively. $N_\alpha^s(\xi)$, $u(Q_\alpha^s)$ and $q(Q_\alpha^s)$ are the shape function, potential and normal flux estimated at the $\alpha^{\text{th}}$ source node in the dual interpolation element, respectively. $N_\beta^v(\xi)$, $u(Q_\beta^v)$ and $q(Q_\beta^v)$ are likewise the shape function, potential and flux evaluated at the $\beta^{\text{th}}$ virtual node, respectively. In this study, the virtual nodal parameters $u(Q_\beta^v)$ and $q(Q_\beta^v)$ are not independent physical quantities, we use the second-layer interpolation to determine their relations to the potential $u$ and normal flux $q$ at the source nodes.

### 2.3. Second-layer interpolation

The MLS approximation is applied for the second-layer interpolation, which is used to construct the relations between the source and virtual nodes. Additional constraint equations are required to condense the degrees of freedom at virtual nodes. The second-layer interpolations for values at the virtual nodes are expressed as:

$$u(Q_\beta^v) = \sum_{m=1}^{M^\beta} \phi_m^{vs}(\xi_\beta^v)u(Q_{m(\beta)}^s), \tag{6}$$

$$q(Q_\beta^v) = \sum_{m=1}^{M^\beta} \phi_m^{vs}(\xi_\beta^v)q(Q_{m(\beta)}^s), \tag{7}$$

where $M^\beta$ denotes the total number of source nodes $Q_{m(\beta)}^s$ covered in the influence domain of virtual node $Q_\beta^v$, $\phi_m^{vs}(\xi_\beta^v)$ is the shape function of the MLS approximation corresponding to source node $Q_m^s$, $u(Q_{m(\beta)}^s)$ and $q(Q_{m(\beta)}^s)$ are potential and flux of source node $Q_{m(\beta)}^s$, and the $\xi_\beta^v$ is the parametric coordinate of virtual node $Q_\beta^v$. The details of the interpolation functions in Eqs. (6) and (7) and the MLS approximation are available in Ref. [22], Ref. [27], respectively.

Substituting Eq. (6) into Eq. (4) yields the formulation for the potential:

$$u(\xi) = \sum_{\alpha=1}^{n\alpha} N_\alpha^s(\xi)u(Q_\alpha^s) + \sum_{\beta=1}^{n\beta}\sum_{m=1}^{M^\beta} N_\beta^v(\xi)\phi_m^{vs}(\eta_\beta^v)u(Q_{m(\beta)}^s) = \sum_{j=1}^{K} \overline{N_j^s}(\xi)u(Q_j^s), \tag{8}$$

and substituting Eq. (7) into Eq. (5) yields the formulation for the normal flux:

$$q(\xi) = \sum_{\alpha=1}^{n\alpha} N_\alpha^s(\xi)q(Q_\alpha^s) + \sum_{\beta=1}^{n\beta}\sum_{m=1}^{M^\beta} N_\beta^v(\xi)\phi_m^{vs}(\eta_\beta^v)q(Q_{m(\beta)}^s) = \sum_{j=1}^{K} \overline{N_j^s}(\xi)q(Q_j^s), \tag{9}$$

where $K$ is equal to the sum of the number of source nodes $Q_{m(\beta)}^s$ covered in the influence domain of virtual node $Q_\beta^v$ and the number of the dual

interpolation element's source nodes $Q_\alpha^s$ minus the number of coincident source nodes.

## 3. DiGBFM

### 3.1. Discretization of the BIE for potential problems

Consider the steady-state potential problem in an arbitrary 2-D finite domain Ω with the boundary Γ. The problem can be described in a boundary integral equation form, the dis cretization form of the BIE for a source point $P$ can be written as:

$$c(P)u(P) = \int_\Gamma u^*(P,Q)q(Q)d\Gamma(Q) - \int_\Gamma q^*(P,Q)u(Q)d\Gamma(Q), \qquad P,Q \in \Gamma \tag{10}$$

where the coefficient $c(P)$ is defined as:

$$c(P) = \begin{cases} 1 & \text{P in the internal domain} \\ \frac{1}{2} & \text{P on the smooth boundary} \\ 0 & \text{P in the outer domain} \end{cases} \tag{11}$$

and $u(Q)$ denotes the potential and $q(Q)$ denotes the flux at the boundary point $Q$ on Γ, respectively. $u^*(P, Q)$ is the fundamental solution, and $q^*(P, Q)$ is the normal derivative of $u^*(P, Q)$. We have for 2-D potential problems:

$$\begin{aligned} u^*(P,Q) &= -\frac{1}{2\pi}\ln r \\ q^*(P,Q) &= \frac{\partial u^*(P,Q)}{\partial r} \\ r &= |P-Q| \end{aligned} \tag{12}$$

where r is the distance between the source node $P$ and the field point $Q$.

Consider a set of discrete points $Q_j, j = 1,2\ldots n$ on the boundary Γ. The potential $u(Q)$ and its flux $q(Q)$ are approximated by functions $\overline{N_j^s}(Q_{(\xi)})$:

$$\begin{cases} u(Q_{(\xi)}) = \sum_{j=1}^{n} \overline{N_j^s}(Q_{(\xi)})u(Q_j^s) \\ q(Q_{(\xi)}) = \sum_{j=1}^{n} \overline{N_j^s}(Q_{(\xi)})q(Q_j^s) \end{cases} \tag{13}$$

Substituting Eq. (13) into Eq. (10) leads to:

$$c(P)u(P) = \sum_{j=1}^{n} G_j(P)q(Q_j^s) - \sum_{j=1}^{n} H_j(P)u(Q_j^s) \tag{14}$$

where

$$\begin{aligned} G_j(P) &= \int_\Gamma u^*(P,Q)\overline{N_j^s}(Q_{(\xi)})d\Gamma(Q) \\ H_j(P) &= \int_\Gamma q^*(P,Q)\overline{N_j^s}(Q_{(\xi)})d\Gamma(Q) \end{aligned} \tag{15}$$

Applying the Galerkin method to Eq. (14) with respect to the boundary nodes $P_i$, one has:

$$\sum_{j=1}^{n} C_{Gij}u(Q_j^s) = \sum_{j=1}^{n} G_{Gij}^{uu}q(Q_j^s) - \sum_{j=1}^{n} G_{Gij}^{qu}u(Q_j^s) \tag{16}$$

where the entries of the coefficients in Eq. (16) are defined as follows:

$$G_{Gij}^{uu} = \int_\Gamma \overline{N_i^s}(P_{(\xi)})\left[\int_\Gamma u^*(P,Q)\overline{N_j^s}(Q_{(\xi)})d\Gamma(Q)\right]d\Gamma(P) \tag{17}$$

$$G_{Gij}^{qu} = \int_\Gamma \overline{N_i^s}(P_{(\xi)})\left[\int_\Gamma q^*(P,Q)\overline{N_j^s}(Q_{(\xi)})d\Gamma(Q)\right]d\Gamma(P) \tag{18}$$

$$C_{Gij} = \frac{1}{2}\int_\Gamma \overline{N_i^s}(P_{(\xi)})\overline{N_j^s}(P_{(\xi)})d\Gamma(P) \tag{19}$$

in which $c(P)$is set equal to $\frac{1}{2}$ for P lying on the boundary. Subscript 'G' expresses the quantities related to the Galerkin method.

To make the derivation procedure facilitative, Eq. (16) is written in a matrix form as:

$$\mathbf{H}_G\mathbf{u} = \mathbf{G}_G\mathbf{q} \tag{20}$$

in which $\mathbf{H}_G$ contains terms in Eqs. (18) and (19), while $\mathbf{G}_G$represents the term in Eq. (17).

### 3.2. Solution for potential problems

To achieve symmetry, firstly multiplying Eq. (20) by $\mathbf{G}_G$ and $\mathbf{H}_G{}^T$ respectively, one gets:

$$\mathbf{D}_G^{GH}\mathbf{u} = \mathbf{D}_G^{GG}\mathbf{q} \tag{21}$$

and

$$(\mathbf{D}_G^{GH})^T\mathbf{q} = \mathbf{D}_G^{HH}\mathbf{u} \tag{22}$$

where $\mathbf{D}_G^{GG} = \mathbf{G}_G\mathbf{G}_G$, $\mathbf{D}_G^{GH} = \mathbf{G}_G\mathbf{H}_G$, and $\mathbf{D}_G^{HH} = \mathbf{H}_G^T\mathbf{H}_G$.

It is obvious that both $\mathbf{D}_G^{GG}$ and $\mathbf{D}_G^{HH}$ are symmetric matrices.

Afterward, Eq. (21) is adopted to all segments of the boundary $\Gamma_1$ with prescribed potential, while Eq. (22) is adopted to all segments of the boundary $\Gamma_2$ with prescribed flux. Partitioning matrices$\mathbf{D}_G^{GG}$, $\mathbf{D}_G^{GH}$ and $\mathbf{D}_G^{HH}$ with respect to boundaries $\Gamma_1$ and $\Gamma_2$ respectively, one can get:

$$[\mathbf{D}_{G11}^{GH}, \mathbf{D}_{G12}^{GH}]\begin{Bmatrix}\mathbf{u}_1\\ \mathbf{u}_2\end{Bmatrix} = [\mathbf{D}_{G11}^{GG}, \mathbf{D}_{G12}^{GG}]\begin{Bmatrix}\mathbf{q}_1\\ \mathbf{q}_2\end{Bmatrix}, \tag{23}$$

and

$$\left[(\mathbf{D}_{G12}^{GH})^T, (\mathbf{D}_{G22}^{GH})^T\right]\begin{Bmatrix}\mathbf{q}_1\\ \mathbf{q}_2\end{Bmatrix} = [\mathbf{D}_{G21}^{HH}, \mathbf{D}_{G22}^{HH}]\begin{Bmatrix}\mathbf{u}_1\\ \mathbf{u}_2\end{Bmatrix}, \tag{24}$$

where subscripts '1' and '2'express variables at boundary $\Gamma_1$ and $\Gamma_2$ respectively.

By moving the unknown physical variables to the left-hand side and known physical variables to the right-hand side, and then combing the rearranged Eqs. (23) and (24), finally, a standard system of linear equations can be expressed as:

$$\begin{bmatrix}\mathbf{D}_{G11}^{GH} & \mathbf{D}_{G12}^{GH}\\ -\mathbf{D}_{G21}^{HH} & -\mathbf{D}_{G22}^{HH}\end{bmatrix}\begin{Bmatrix}\mathbf{u}_1\\ \mathbf{u}_2\end{Bmatrix} = \begin{bmatrix}\mathbf{D}_{G11}^{GG} & \mathbf{D}_{G12}^{GG}\\ -(\mathbf{D}_{G12}^{GH})^T & -(\mathbf{D}_{G22}^{GH})^T\end{bmatrix}\begin{Bmatrix}\mathbf{q}_1\\ \mathbf{q}_2\end{Bmatrix} \tag{25}$$

which is equivalent to:

$$\begin{bmatrix}-\mathbf{D}_{G11}^{GG} & \mathbf{D}_{G12}^{GH}\\ (\mathbf{D}_{G12}^{GH})^T & -\mathbf{D}_{G22}^{HH}\end{bmatrix}\begin{Bmatrix}\mathbf{q}_1\\ \mathbf{q}_2\end{Bmatrix} = \begin{bmatrix}-\mathbf{D}_{G11}^{GH} & \mathbf{D}_{G12}^{GG}\\ \mathbf{D}_{G21}^{HH} & -(\mathbf{D}_{G22}^{GH})^T\end{bmatrix}\begin{Bmatrix}\mathbf{u}_1\\ \mathbf{q}_2\end{Bmatrix} \tag{26}$$

Eq. (25) can be expressed in a generic form:

$$\mathbf{A}\mathbf{x} = \mathbf{b} \tag{27}$$

where $\mathbf{A}$ is the coefficient matrix, $\mathbf{x}$ is the unknown vector, and $\mathbf{b}$ is the right-hand side vector in Eq. (26). As both $\mathbf{D}_G^{GG}$ and $\mathbf{D}_G^{HH}$ are symmetric, the left-hand side matrix in Eq. (26), or $\mathbf{A}$matrix in Eq. (27), is symmetric. We note that the symmetry is achieved here by simply using matrix manipulations, without the need to apply the hypersingular BIE as in the traditional Galerkin BEM.

## 4. Numerical examples and discussions

In this section, we present four numerical examples to demonstrate the accuracy and convergence of the proposed DiGBFM in solving 2-D potential problems.

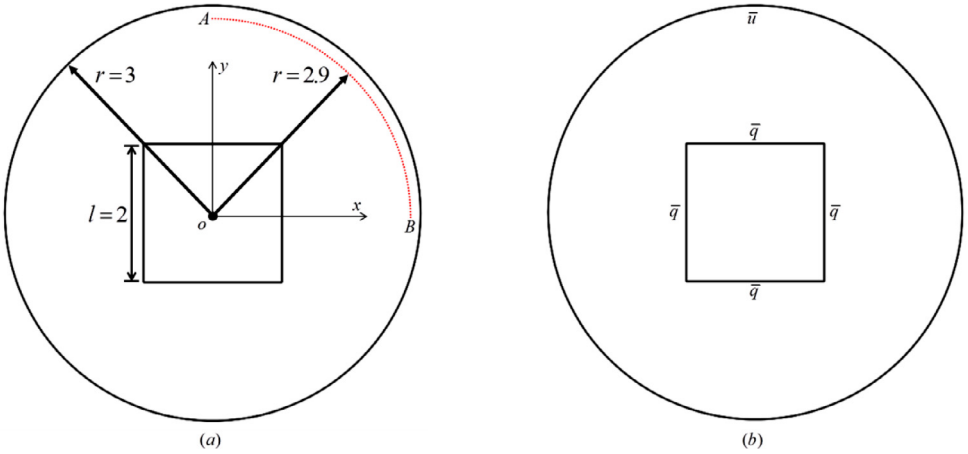


**Fig. 2.** Mixed problem on simple geometry: (a) geometric model and (b) boundary conditions.

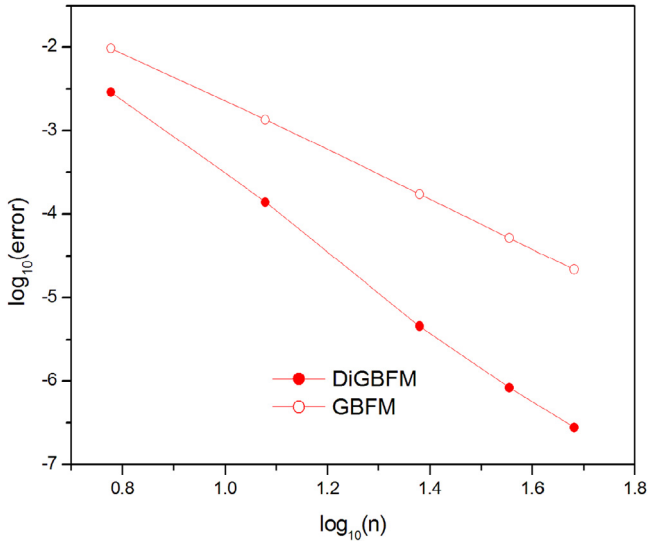


**Fig. 3.** Relative errors and convergence rates of $u$ along all straight lines.

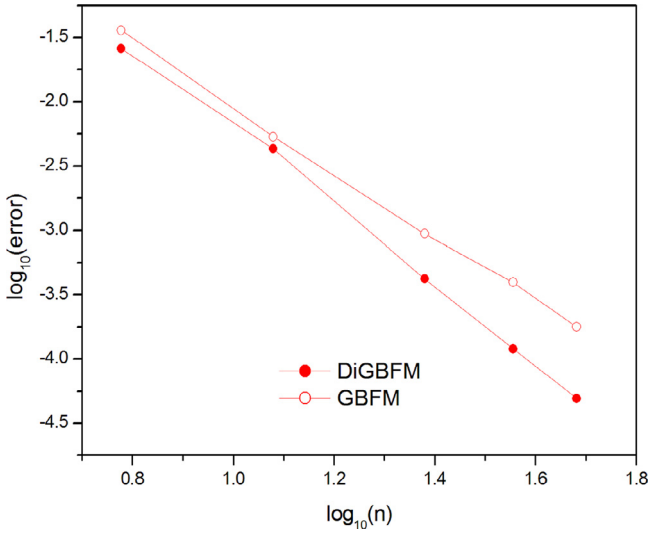


**Fig. 4.** Relative errors and convergence rates of $q$ along the circle.

### 4.1. Example 1

We first consider a problem with mixed boundary conditions (BCs) on a simple geometry. The size of the geometry is illustrated in Fig. 2(a) (with length units in mm), which is a circle region with a center cut made of four straight lines. The analytical solution used in this problem is given by:

$$u(x, y) = -x^4 - y^4 + 6x^2y^2$$

The prescribed $u$ and $q$ values based on the above solution along all boundaries are shown in Fig. 2(b). The Dirichlet boundary condition on the circle and Neumann boundary conditions on all inner straight edges are imposed according to the above analytical solution. To study the convergence and accuracy of the proposed method, we employed five sets of source nodes on all straight lines, $n$ = 6, 12, 24, 36, and 48. The number of source nodes on the circle is six times more than the nodes on any straight line.

Figs. 3 and 4 show the relative errors for $u$ on inner edges with Neumann boundary conditions and $q$ on outer edge with Dirichlet boundary conditions, respectively, where GBFM is the regular Galerkin BFM. Combined with the exact solution, the numerical results of $u$ and $q$ inside the domain along the curve AB are shown in Figs. 5 and 6, respectively. As illustrated in Figs. 3–6, high accuracy and convergence rates for the mixed problem with this relatively simple geometry can be achieved using the proposed DiGBFM.

The effect of the parameter $d$ in Eqs. (2) and (3) on the computational accuracy of the proposed method has been studied in this example. The above five sets of source nodes are also used here. As shown in Figs. 7 and 8, for the same number of source nodes, the accuracy of the DiGBFM will be slightly decreased with the increment of the parameter $d$. It can be inferred that the best parameter $d$ should be taken between 0.15 and 0.2.

### 4.2. Example 2

A complicated geometry, which consists of three identical leaf-like regions equally spaced within a circle, is considered for the second example. The dimensions of the geometry is shown in Fig. 9. An analytical solution for the 2-Dpotential problem is selected as:

$$u(x, y) = -x^3 - y^3 + 3x^2y + 3xy^2.$$

Dirichlet boundary condition is imposed on all edges of the domain in accordance with the above analytical solution. Fig. 10 shows the number of source nodes on each edge. We employed five sets of source nodes on interior circular edge, $n$ = 6, 12, 24, 48, and 60. The number of source nodes on all interior edges is $7n$, and the number of source nodes on all exterior edges is $30n$.

Fig. 11 shows the relative errors and convergence rates of solved $q$ on the boundary.

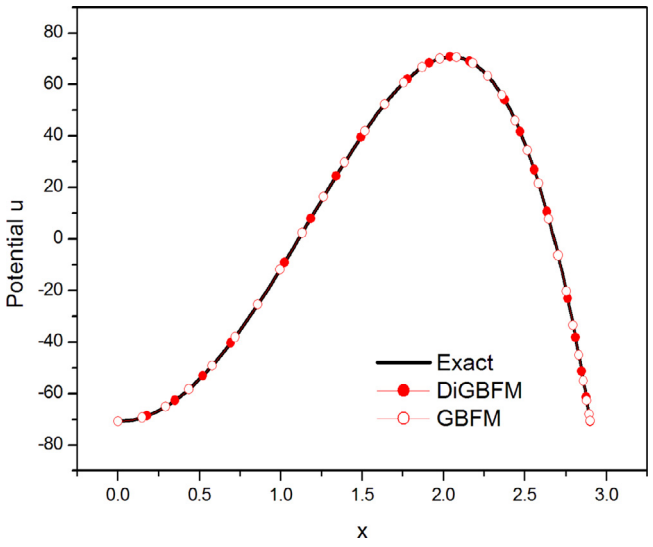


**Fig. 5.** Values of $u$ along the curve AB.

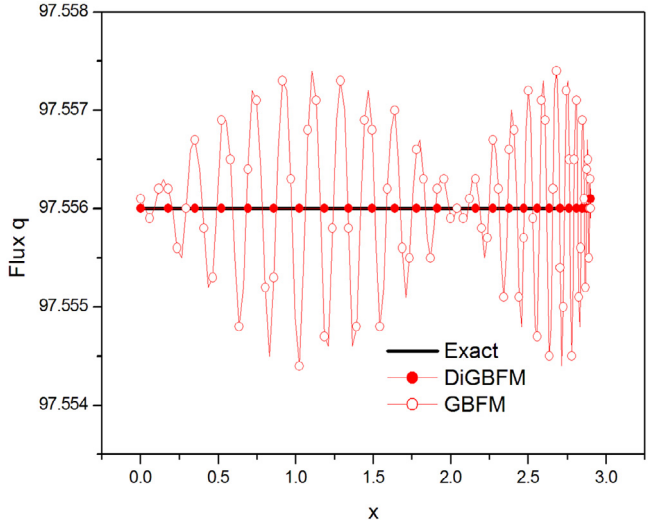


**Fig. 6.** Values of $q$ along the curve AB.

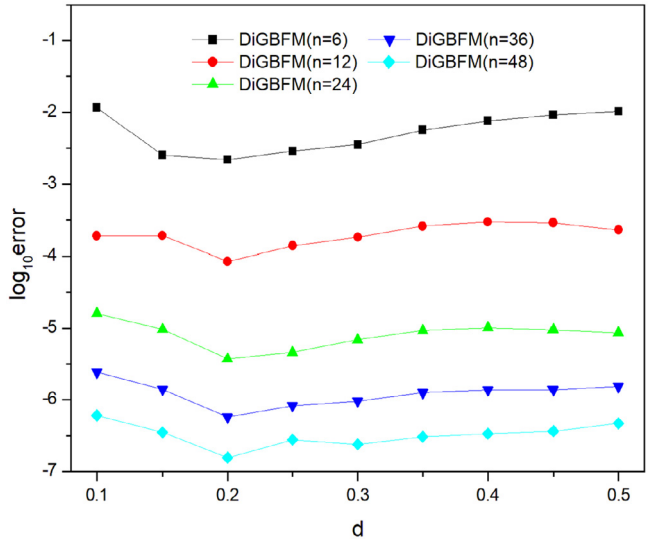


**Fig. 7.** Effect of $d$ on the accuracy of $u$ along all straight lines.

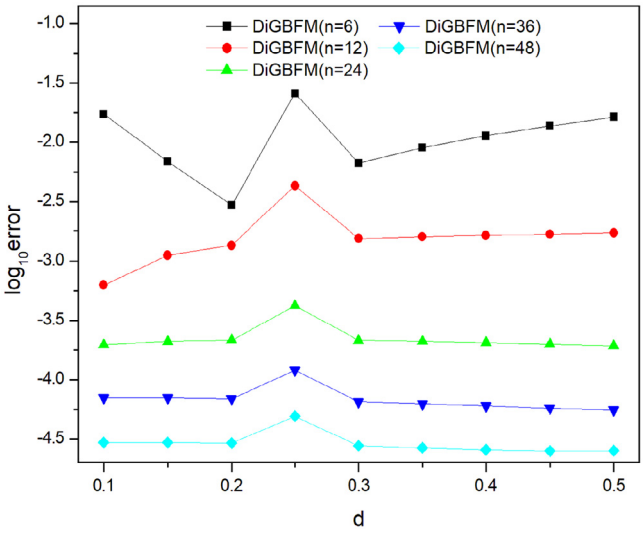


**Fig. 8.** Effect of $d$ on the accuracy of $q$ along the circle.

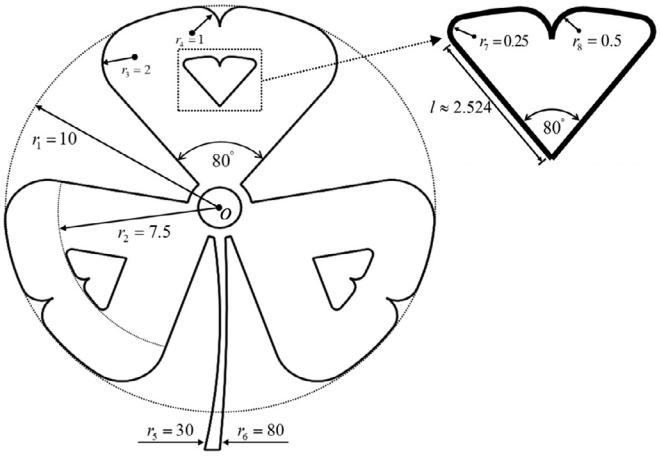


**Fig. 9.** Dirichlet problem on complicated geometry (unit = mm).

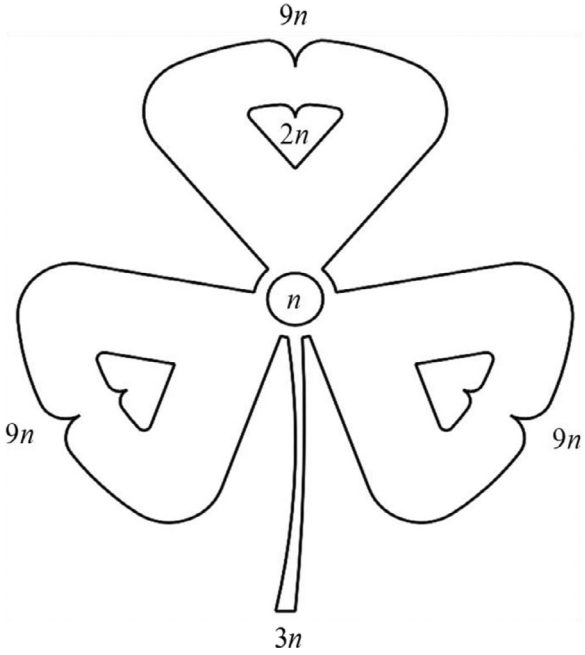


**Fig. 10.** The number of source nodes on each edge.

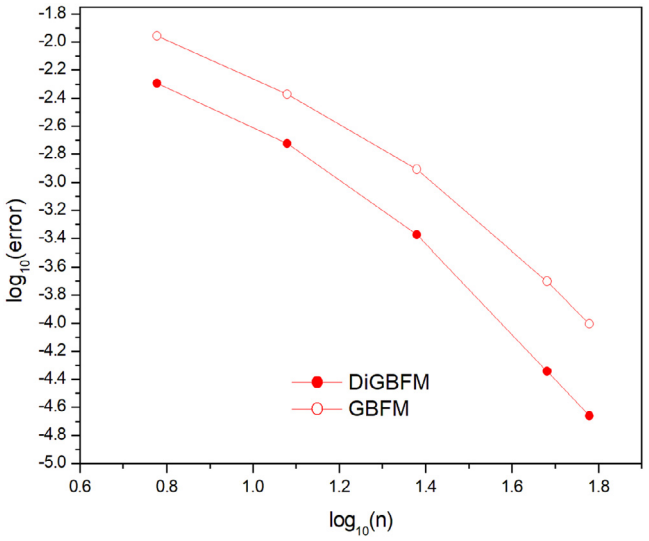


**Fig. 11.** Relative errors and convergence rates of $q$ on all edges.

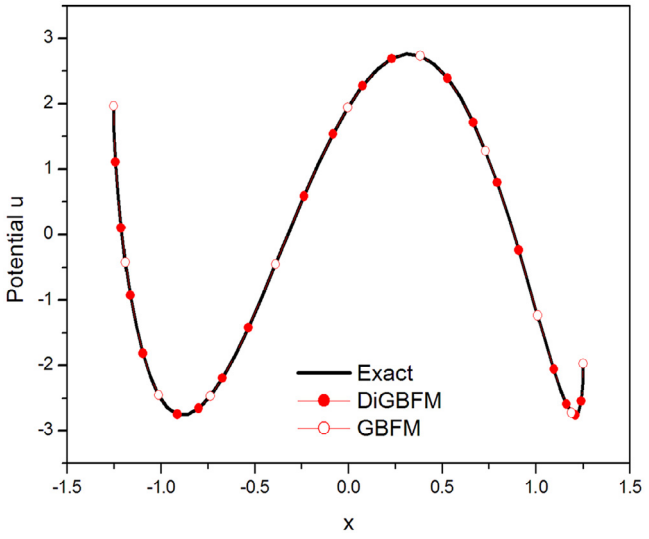


**Fig. 12.** Values of $u$ along a circle of radius 1.25mm centered at the origin.

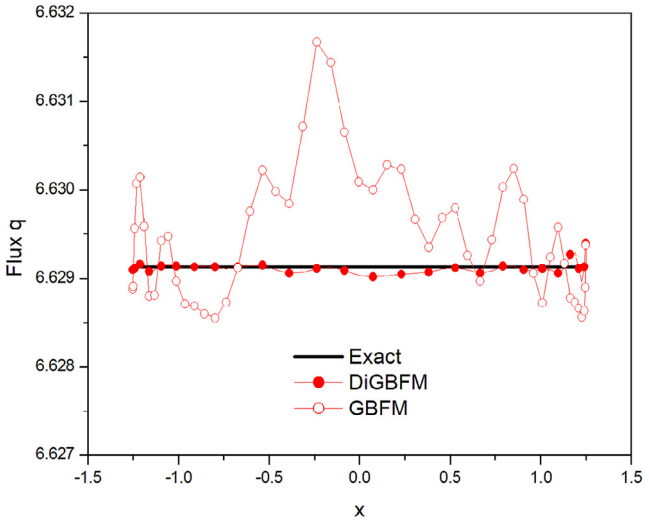


**Fig. 13.** Values of $q$ along the circle of radius 1.25mm centered at the origin.

**Table 1**
Number of elements and source nodes in example 4.

| | DiGBFM | | FEM | | |
|---|---|---|---|---|---|
| | 1 | 2 | 1 | 2 | 3 |
| Elements | 304 | 634 | 742 | 1628 | 288050 |
| Source nodes | 912 | 1902 | 1725 | 3635 | 581757 |

Figs. 12 and 13 show the numerical results of $u$ and $q$ as compared with the exact solution, respectively, which are inside the domain along a circle (angle from $\pi$ to 0) of radius 1.25 mm, centered at the origin.

Since the uncomforting quadratic elements were used in our proposed method, it can achieve higher accuracy and faster convergence rates for the cubic Dirichlet problem with a complicated geometry.

### 4.3. Example 3

A fish-shaped geometry (see Fig. 14) is considered for the third example. The analytical solution used is given by:

$$u(x, y) = x^2 - y^2 + x - y.$$

The prescribed $u$ and $q$ values along all boundaries are shown in Fig. 15. Dirichlet boundary condition is imposed on all edges except for edges of the diamonds according to the above analytical solution.

Fig. 16 shows the number of source nodes on each edge. In this example, there are five sets of source nodes on each interior edge, $n = 4$, 8, 16, 24, 48. The number of source nodes on all exterior edges is 48 times than the nodes on any of the interior edges.

Figs. 17 and 18 show the relative errors and convergence rates of $u$ on the Neumann boundary conditions and $q$ on Dirichlet boundary conditions, respectively.

Fig. 19, shows the numerical results of the potential $u$ along the center line $AB$ shown in Fig. 14.

The results show that DiGBFM has high rates of convergence. The agreement between numerical and exact results is excellent.

### 4.4. Example 4

A forth example is presented to show the accuracy and convergence of the DiGBFM as compared with the FEM. In this example, the model is a $10 \times 10$ square domain with many internal cavities (see Fig. 20(a)), and with the prescribed $u$ along all boundaries as shown in Fig. 20(b).

In the DiGBFM, the potentials and normal fluxes on the boundary are approximated by nonconforming quadratic dual interpolation elements, while these potentials and normal fluxes are approximated by quadratic triangle elements in the FEM. Table 1 lists the number of elements and source nodes for the proposed DiGBFM and FEM.

In the following figures for this example, the results of DiGBFM-912 and DiGBFM-1902 are obtained by the proposed method using 912 and 1902 source nodes, respectively. The FEM results with 1725, 3635 and 581757 source nodes are denoted by FEM-1725, FEM-3635 and FEM-581757, respectively. The numerical results by the FEM with 581757 source nodes are used as reference solution.

The numerical results of the potential along a line (x = 5.0 mm) are shown in Fig. 21, and the potential distribution over the entire domain is shown in Fig. 22. From Fig. 21, one can see that as the number of the source nodes increases, the numerical results of the potential calculated by both methods approach to the reference solution.

### 4.5. Example 5

The fifth example is a steady heat conduction problem on a real dam model (see Fig. 23). The bottom of the dam is 49 m. The left and right sides of the real dam model are adjacent to the upstream and downstream, respectively. Besides, the upstream water level is 65 m. The other edges are exposed to air.

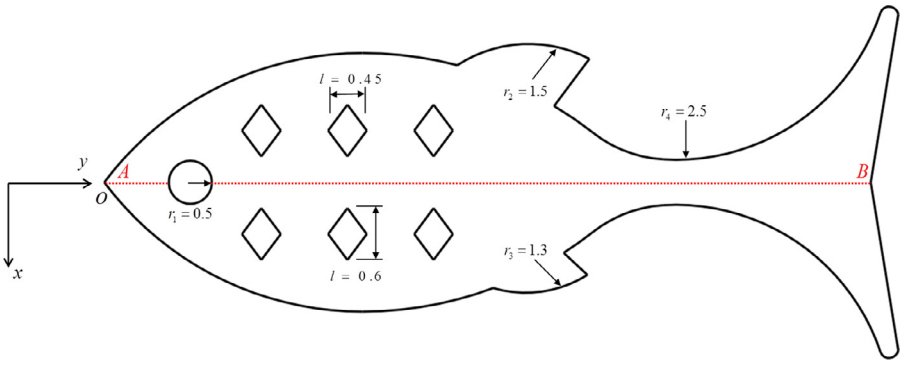


**Fig. 14.** Mixed problem with a fish shape geometry: geometric model.

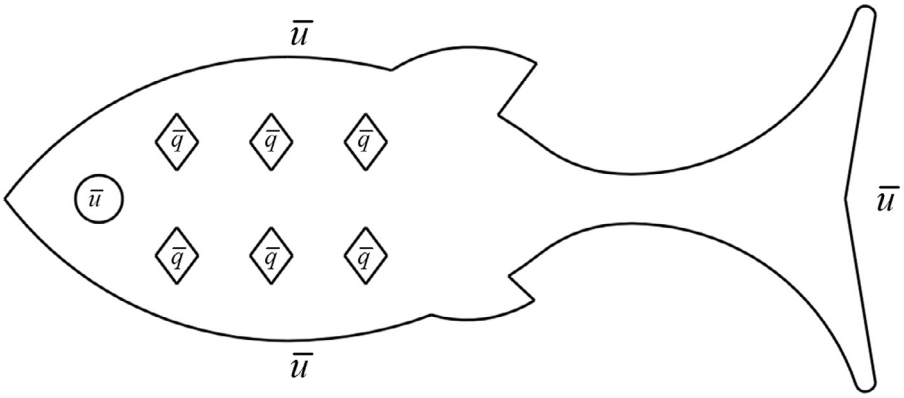


**Fig. 15.** Mixed problem with a fish shape geometry: boundary conditions.

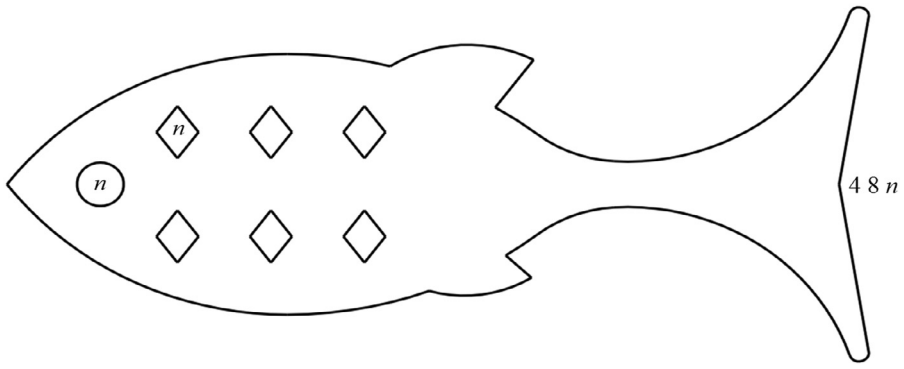


**Fig. 16.** The number of source nodes on each edge.

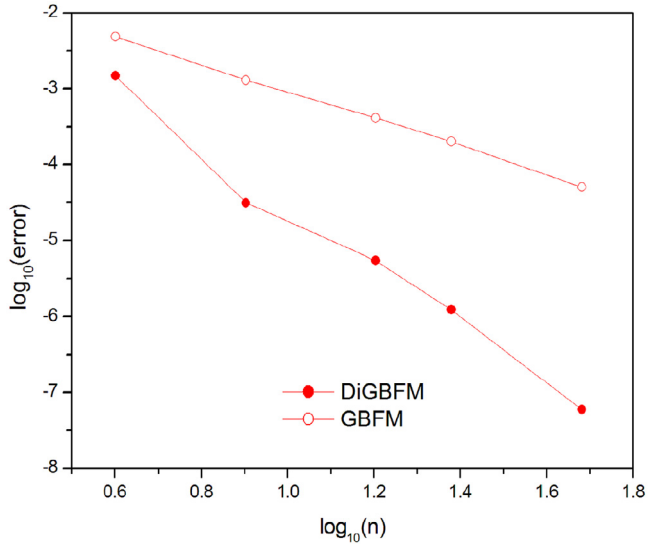


**Fig. 17.** Relative errors and convergence rates of $u$ on interior diamond edges.

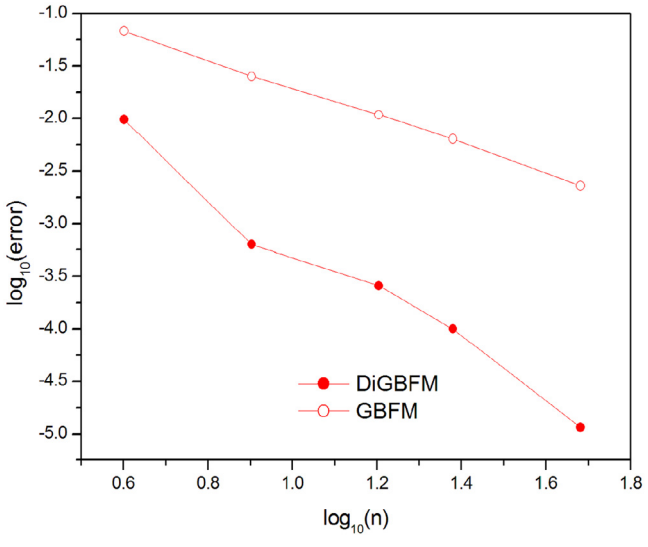


**Fig. 18.** Relative errors and convergence rates of $q$ on other edges.

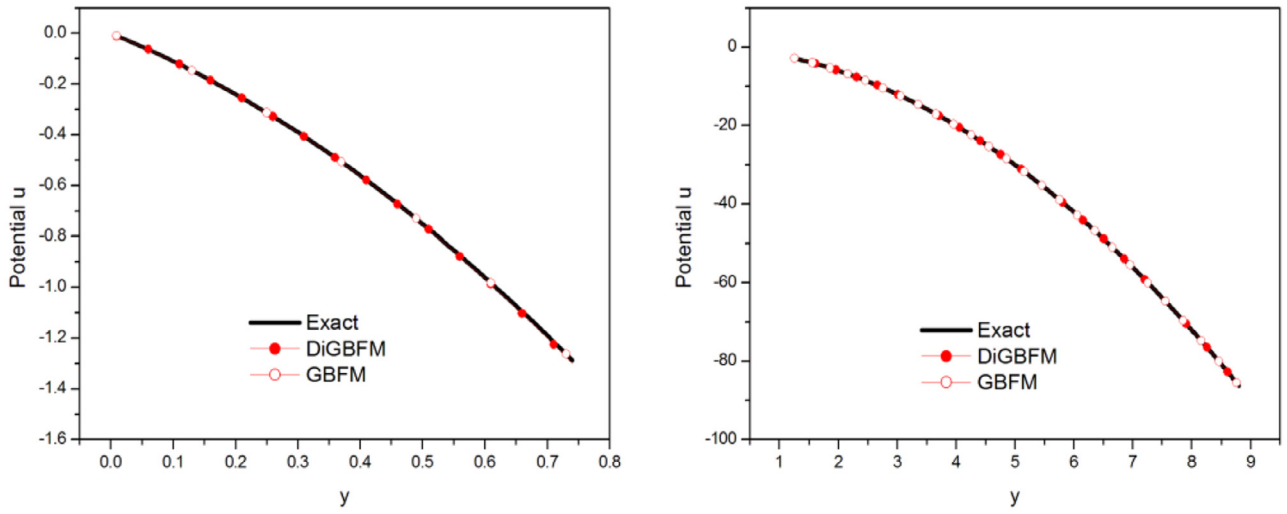


**Fig. 19.** Values of u along the line *AB*.

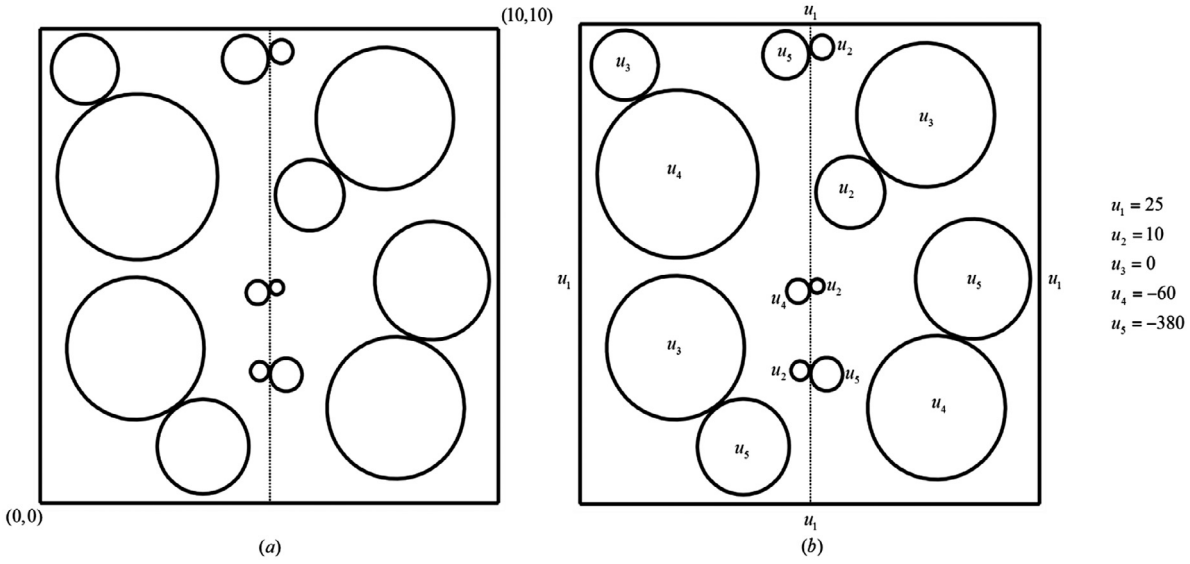


**Fig. 20.** A mixed problem on a square domain with internal cavities: (a) geometry and (b) boundary conditions.

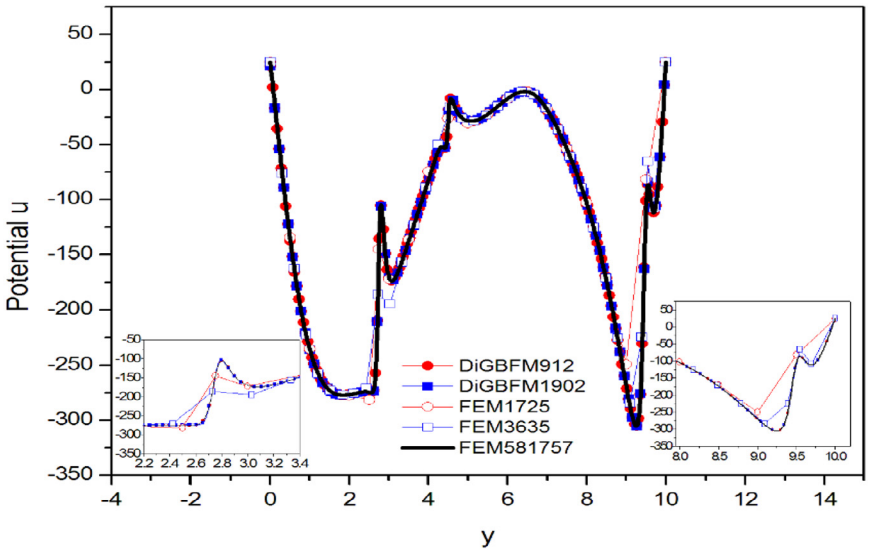


**Fig. 21.** Values of potential $u$ along the line $x = 5$mm.

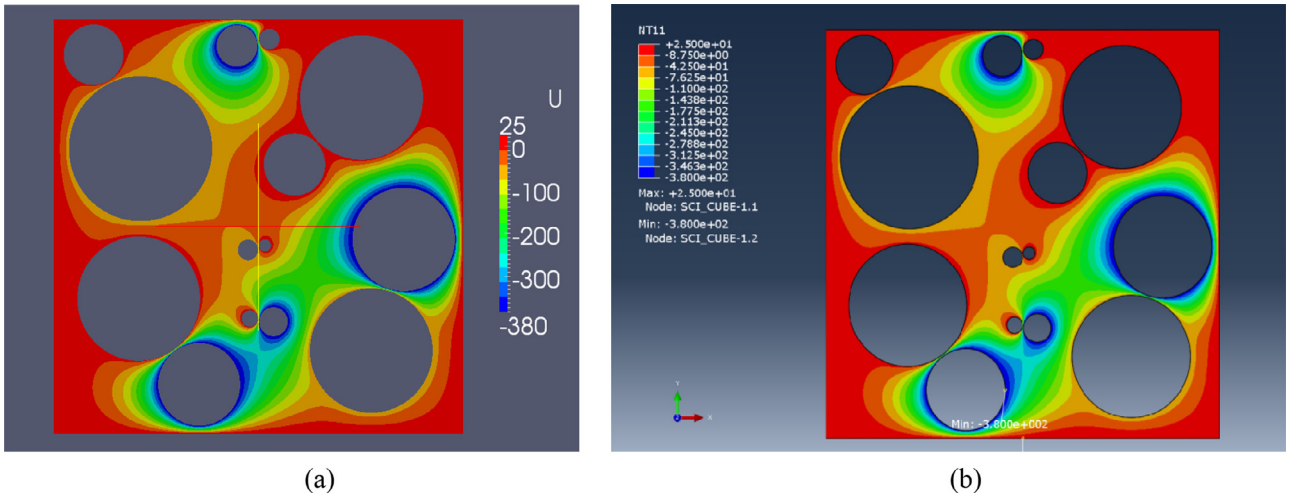


**Fig. 22.** Potential distribution computed by: (a) DiGBFM with 1902 source nodes and (b) FEM with 581757 nodes.

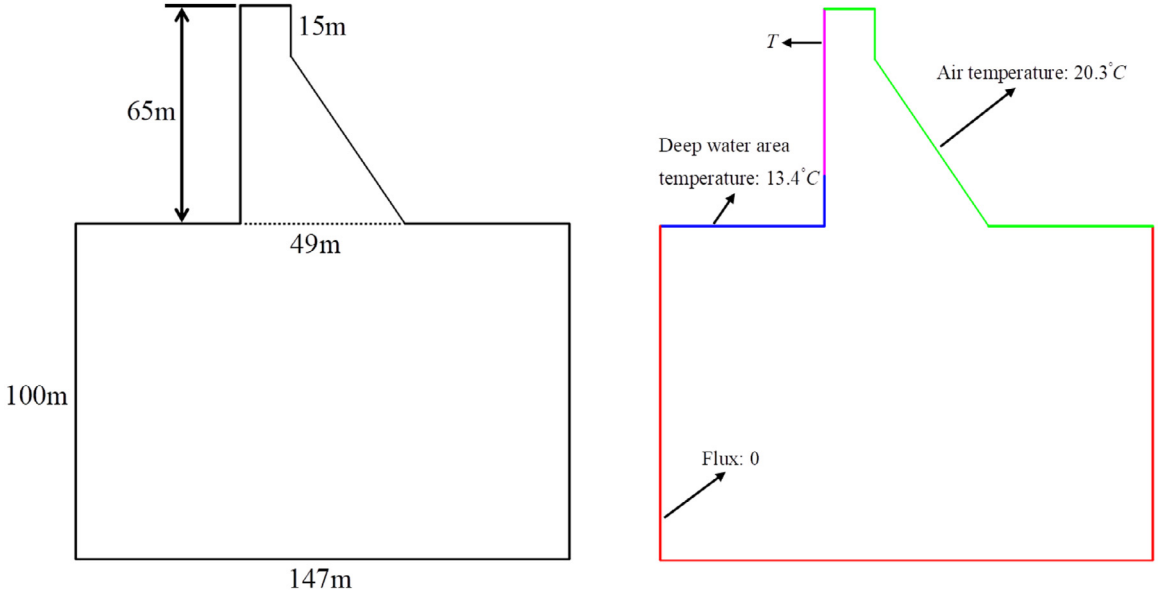


**Fig. 23.** Steady heat conduction problem on a dam: (a) geometry and (b) boundary conditions.

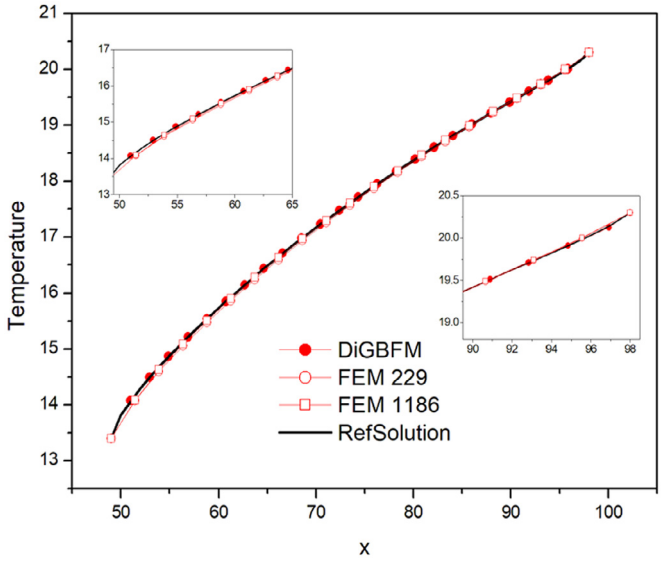


**Fig. 24.** Temperature along the interface between the bed rock and the dam.

The edges of the bed rock are adiabatic except for the top and the local temperature is 20.3 °C (see Fig. 23). Moreover, the temperature of water at the depth more than 50 meters is taken as 13.4 °C, while the temperature of water within 50 m is given by:

$$T = 20.3 - 0.138 \times h$$

where $h$ is the depth into the water.

In the following figures for this example, the results of DiGBFM is obtained by the proposed method using 60 source nodes. The FEM results with 229, 1186 source nodes are denoted by FEM 229, FEM 1186, respectively. The result obtained by the FEM with 165895 source nodes is used as reference solution, which is denoted as RefSolution. The temperature along the bottom of the dam is shown in Fig. 24.

## 5. Conclusions

In this paper, considering the broader application prospect of the traditional symmetric Galerkin boundary element method in the field of time domain potential problems and elastodynamic problems, by combining the dual interpolation method and the symmetric Galerkin BEM approach, a dual interpolation symmetric Galerkin boundary face method (DiGBFM) is applied for solving 2-D steady-state potential prob-

lems. The new method is a generalization of the Galerkin and the dual interpolation BFM and inherits the advantages from both of them. Compared with the traditional symmetric Galerkin BEM, the DiGBFM can be adopted to readily and accurately approximate both continuous and discontinuous fields and no need to use the hypersingular BIEs, therefore, traditional symmetric Galerkin BEM is more difficult than DiGBFM. Numerical examples with different geometries and type of boundary conditions have been presented to demonstrate the convergence and accuracy of the DiGBFM and verify the feasibility of combining the dual interpolation method with the symmetric Galerkin BEM approach.

Extensions of the DiGBFM to solving 3-D potential and elastostatic problems are possible, because of the advantages of DiGBFM: improve the accuracy of the interpolation calculation and mitigate the ponderous task of mesh generation, it also has the potential to increase the accuracy when it is applied to elasticity or other difficult problems. By coupling DiGBFM with the fast multipole method, since no geometric errors are introduced, a truly seamless interaction between CAD and CAE can be achieved no matter how coarse the discretization is and DiGBFM may be applied to solve large-scale problems with even more complicated geometries. Work along this line is underway.

## Acknowledgments

This work was supported by the National Natural Science Foundation of China under grant number 11772125 and 11472102.

## References

[1] Mukherjee S. Boundary element methods in creep and fracture. New York: Applied Science Publishers; 1982.
[2] Brebbia CA, Dominguez J. Boundary elements - an introductory course. New York: McGraw-Hill; 1989.
[3] Banerjee PK. The boundary element methods in engineering. 2nd ed. New York: McGraw-Hill; 1994.
[4] Bonnet M. Boundary integral equation methods for solids and fluids. Chichester: Wiley; 1995.
[5] Liu YJ. Fast multipole boundary element method - theory and applications in engineering. Cambridge: Cambridge University Press; 2009.
[6] Cruse TA. Boundary element analysis in computational fracture mechanics. Dordrecht, The Netherlands: Kluwer Academic Publishers; 1988.
[7] Xie GZ, Zhang JM, Cheng H. A direct traction boundary integral equation method for three-dimension crack problems in infinite and finite domains. Comput Mech 2014;53(4):575–86.
[8] Zhang YM, Gu Y, Chen JT. Stress analysis for multilayered coating systems using semi-analytical BEM with geometric non-linearities. Comput Mech 2011;47(5):493–504.
[9] Dong CY, Yang X, Pan E. Analysis of cracked transversely isotropic and inhomogeneous solids by a special BIE formulation. Eng Anal Bound Elem 2011;35(2):200–6.
[10] Liu YJ, Li YX, Xie W. Modeling of multiple crack propagation in 2-D elastic solids by the fast multipole boundary element method. Eng Fract Mech 2017;172:1–16.
[11] Chidgzey SR, Trevelyan J, Deeks AJ. Coupling of the boundary element method and the scaled boundary finite element method for computations in fracture mechanics. Comput Struct 2008;86:1198–203.
[12] Wang XH, Zhang JM, Zhou FL. An adaptive fast multipole boundary face method with higher order elements for acoustic problems in three-dimension. Eng Anal Bound Elem 2013;37:114–52.
[13] Yan F, Pan PZ, Feng XT, Li SJ, Jiang Q. A novel fast overrelaxation updating method for continuous-discontinuous cellular automaton. Appl Math Model 2019;66:156–74.
[14] Yan F, Pan PZ, Feng XT, Li SJ. The continuous-discontinuous cellular automaton method for elastodynamic problems. Eng Fract Mech 2018;204:482–96.
[15] Zhong BD, Yan F, Lv JH. Continuous-discontinuous hybrid boundary node method for frictional contact problems. Eng Anal Bound Elements 2018;87:19–26.
[16] Gray LJ, Griffith BE. A fast Galerkin boundary integral algorithm. Commun Numer Meth Eng 1998;14:1109–17.
[17] Sirtori S. General stress analysis method by means of integral equations and boundary elements. Mechanica 1979;14:210–18.
[18] Bonner M, Maier G, Polizzotto C. Symmetric Galerkin boundary element methods. Appl Mech Rev 1998;51(11):669–704.
[19] Gray LJ, Chinta Balakrishna, Kane JH. Symmetric Galerkin fracture analysis. Eng Anal Bound Elements 1995;15:103–9.
[20] Phan AV, Napier JAL, Gray LJ, Kaplan T. Symmetric-Galerkin BEM simulation of fracture with frictional contact. Int J Numer Methods Eng 2003;57:835–51.
[21] Zhang JM, Han L, Lin WC, Dong YQ. A new implementation of BEM by an expanding element interpolation method. Eng Anal Bound Elem 2017;78:1–7.
[22] Zhang JM, Lin WC, Dong YQ. A double-layer interpolation method for implementation of BEM analysis of problems in potential theory. Appl Math Model 2017;51:250–69.
[23] Zhang JM, Zhong YD, Dong YQ. Expanding element interpolation method for analysis of thin-walled structures. Eng Anal Bound Elem 2018;86:82–8.
[24] Zhang JM, Qin XY, Han X. A boundary face method for potential problems in three dimensions. Int J Numer Methods Eng 2009;80:320–37.
[25] Qin XY, Zhang JM, Li GY. An element implementation of the boundary face method for 3D potential problems. Eng Anal Bound Elem 2010;34:934–43.
[26] Yu GY, Fan SC. Symmetric BEM formulations for 2-D steady-state and transit potential problems. Comput Struct 2003;81:27–37.
[27] Lancaster P, Salkauskas K. Surface generated by moving least squares methods. Math Comput 1981;37:141–58.